JOURNAL OF MATERIALS SCIENCE 24 (1989) 2497–2502

Free volume conduction and magnetic solitons in polystyrene composites containing transition metals

A. EL-TAWANSI, N. KINAWY, M. EL-MITWALLY
Department of Physics, Faculty of Science, Mansoura University, Mansoura 35516, Egypt

Films (200 to 600 μm thick) of polystyrene composites, containing nickel and cobalt metallic powders, were prepared by a casting method. The micrographical analysis revealed a morphological deformation in the polymeric matrix due to the metallic intrusions. No change in the main transition temperatures was observed by differential scanning calorimetry. The d.c. electrical resistivity and the magnetic susceptibility were measured in the temperature range 300 to 470 K. The electrical resistivity results were interpreted on the basis of the free volume model with protonic charge carriers. The magnetic results revealed a magnetic role of the polymeric matrix due to the collective states of the π-electrons (magnetic solitons) in the presence of the ferromagnetic metallic clusters. An s–d type magnetic interaction was suggested between the ferromagnetic particles and the solitons in the close vicinity of the particle surface.

1. Introduction

Polymerization of polystyrene (PS) was achieved as early as 1839 and it was used as one of the standard examples for the investigation of the glassy state of matter [1]. PS is a preferred material in electronic technology due to its dielectric and mechanical properties and its low cost. PS can be subjected to high temperature and pressure variations, during the manufacture of electronic components [2]. During the last decade numerous publications have been published on the physical properties of PS and its blends with other polymers [3–7].

The present work deals with the effect of nickel and cobalt metallic additives on the electrical and magnetic properties of PS composite films.

2. Experimental procedure

The studied composites were prepared by the following casting method [8]. PS material was dissolved in benzene. After the solution attained a suitable viscosity, the desired metallic powder (particle size $\simeq 50\,\mu$m) was added and the mixture was cast into a glass dish, and kept in a dry atmosphere at 30° C for 2 w. Several thicknesses were available (200 to 600 μm). Differential scanning calorimetry (DSC) was carried out using a thermoanalyser (GDTD 16-Setaram) with a temperature range of − 193 to 1200° C, heating rate of 9° C min^{-1}, and sensitivity 2.5 μV. The magnetic susceptibility was measured using a constructed magnetic pendulum balance of a previously explained Faraday type [9]. The electrical measurements were made by standard techniques [10]. The currrent was measured by an electrometer (Levell TM9 8P) of accuracy $\pm 0.2\%$. The films were in the form of discs of 1.6 $\pm$ 0.001 cm diameter. Contacts were of highly conductive silver paste with an area of 1 cm^2. A guard ring was used. The sample was short circuited for about 2 d, at a constant temperature (300 K), before the d.c. voltage was applied. For the current–voltage and current–temperature dependences, the current was measured in the steady state to avoid errors due to relaxation phenomena.

3. Results and discussion

3.1. Optical microscopy

Figs 1 and 2 show micrographs of the surface of PS composites loaded with 28.6 and 70% nickel powder, respectively. It is clear in Fig. 1 that the presence of metallic clusters results in a morphological deformation in the polymeric matrix. Fig. 2 shows more detailed features which are observed in the polymeric matrix and aligned in a certain direction. A different network is formed in the boundary layer surrounding a filler particle (Fig. 2a). This agrees with the findings of Scheibner and Jäckel [11] for the epoxy resin composite. Following the ideas of Pinheiro and Rosenberg [12], the ends of the main-chain segments are firmly anchored at the filler surface and, therefore, the molecular mobility is reduced at considerable distances from the filler surface. Some holes are observed (Fig. 2b) on the surface of the polymeric matrix which appear to be initiated near individual particles. Such close proximity is to be expected from Goodier's calculations of the highly localized concentration of stress around inclusions [13]. A similar surface morphology was observed in several other highly cross-linked glass polymers [14].

3.2. Thermal analysis

Fig. 3 shows the DSC plots for PS, as pure and as

0022–2461/89 $03.00 + .12

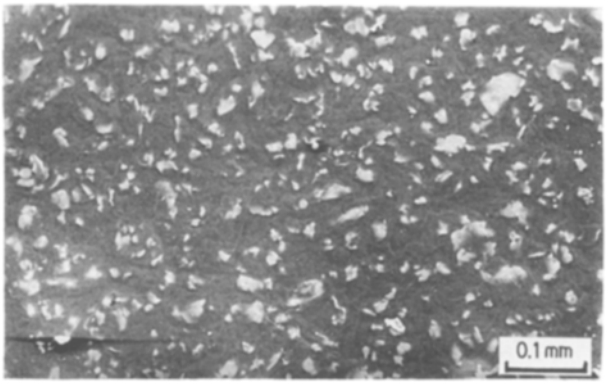

Figure 1 Micrograph of the surface of PS film loaded with 28.6 wt % Ni.

loaded with cobalt and nickel powders. It is noticed that all of the plots mentioned exhibit approximately the same characteristic transition temperatures. This implies that the present additives do not change the main structure of PS. The observed transitions can be assigned as follows.

The T_{gg} endotherms (at 317 to 320 K) may arise from the wagging motion of the phenyl ring [15, 16]. The T_g endotherms (at 345 to 350 K) can be assigned to the glass–rubber transition due to the microBrownian motion of main chain segments, submolecules containing about 50 to 100 C-bonds [17]. At the T_1 endotherms (at 420 to 424 K) the viscoelastic fluid becomes viscous. This transition involves large-scale mobility of large parts of the polymer chains.

3.3. Electrical resistivity

The Arrhenius plots of the d.c. resistivity (ϱ) of the prepared samples, are shown in Figs 4 to 6. The Arrhenius equation is expressed as

$$\varrho = \varrho_0 \exp(E/kT) \quad (1)$$

where ϱ_0 is a constant and E is the apparent activation energy, k is Boltzmann's constant and T is the absolute temperature. An abrupt change in the ϱ-value is observed, for pure PS in Fig. 4, at a critical temperature which corresponds approximately to the glass transition temperature T_g. T_g can usually be identified by the onset of diffusional motion of large chain segments. At temperatures below T_g this motion is hindered by potential energy barriers. With increasing temperature the energy becomes high enough to overcome these barriers, and segmental motion occurs

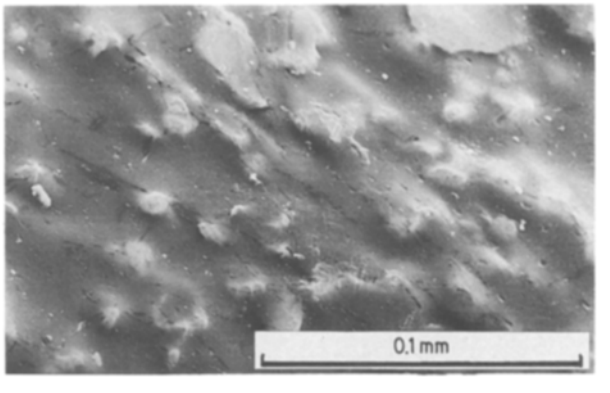

Figure 2 Micrograph of PS loaded with 70% Ni.

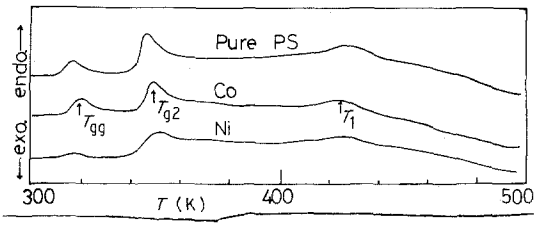

Figure 3 DSC plots for pure PS and PS loaded with 2% Co and Ni.

which results in an increase in the free volume of the system. The increase in free volume would also facilitate the motion of an ionic charge carrier at temperatures above T_g. The Arrhenius plots of PS composites exhibit the same behaviour observed for pure PS. For the sake of clarity in the plots, the polymeric temperature range is only presented in Figs 5 and 6.

Values of the slopes of the Arrhenius plots (and values of ln ϱ measured at 411 K) are plotted, as functions of the weight fraction of metal additives, M, in Figs 7 and 8. As the metallic content increases, up to about 4%, both ln ϱ and E exhibit a relatively sharp increase. Then they decrease for further increases of metallic content. These results may be interpreted on the basis of the free volume model which was suggested previously by Miyamoto and Shibayama [18] for PS and other polymeric films. In this model a theoretical equation for the electrical conductivity was derived in which the free volume, the jump energy, E_j, and the ionic dissociation energy, W, were taken into consideration. Thus the apparent activation energy in Equation 1 was expressed as

$$E = E_h + E_j + W/2\varepsilon \quad (2)$$

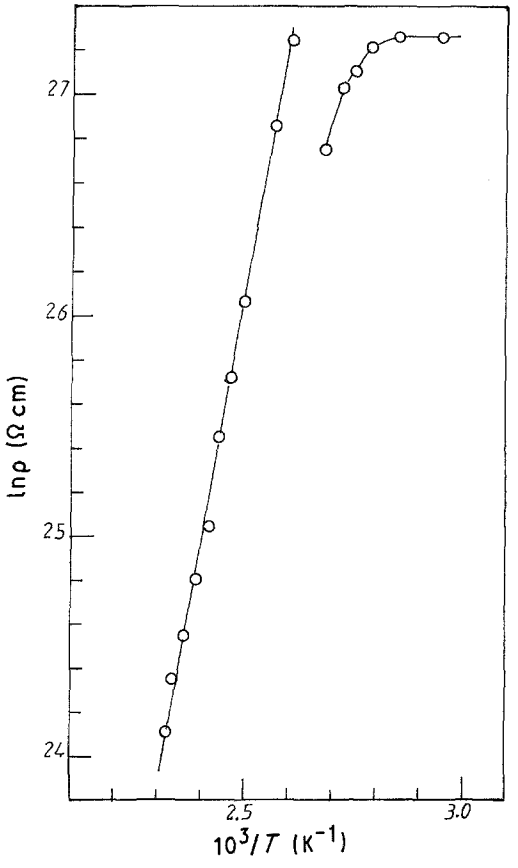

Figure 4 The Arrhenius plots of the d.c. resistivity of PS film.

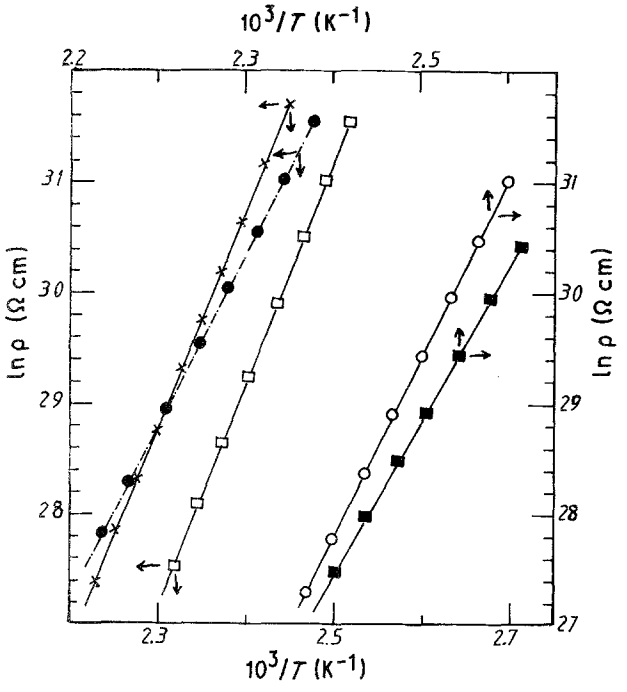

Figure 5 Arrhenius plots for PS loaded with: (●) 2%, (x) 4.5%, (□) 8.5%, (○) 16.5% and (■) 37.5% Ni.

where E_h is the energy of hole formation and ε is the dielectric constant. The critical hole required for transportation of an ion is produced by opposing internal, P_i and external, P, pressure. Thus

$$E_h = (P_i + P)V_i \quad (3)$$

where V_i is the critical hole required for ionic transport. The critical hole formation energy required for transport of ions was finally expressed as

$$E_h = E_a - E_b \quad (4)$$

where E_a and E_b are the apparent activation energies above and below T_g.

The jump energy, E_j, was defined according to the theory of rate process [19] as follows. The probability for jumping into V_i by surmounting the potential barrier E_j is expressed by

$$P_j = \exp(-E_j/kT) \quad (5)$$

The ionic dissociation energy, W, was deduced from the theory of ionic dissociation [20] as follows:

$$n = n_0 \exp(-W/2\varepsilon kT) \quad (6)$$

where n is the concentration of ions and n_0 is a constant. The hybrid energy $E_j + W/2\varepsilon$ was equal to the apparent activation energy (E_b) at temperatures below T_g [18].

The charge carriers may be provided mainly from impurities such as fragments of a polymerization catalyst, absorbed water, and by degradation or dissociation products of the polymer itself. The probable charge carriers in polymers are H^+, Na^+, K^+, etc., as cations and OH^-, Br^-, Cl^-, etc., as anions. H^+ will be the most popular ionic charge carrier in many polymers because it can be provided from absorbed water, hydroxy groups, or carboxy groups attached to the polymer molecules. However, H^+ would be trapped in part, as a lone electron pair, or would become a hydromium ion, H_3O^+, under existing absorbed water.

According to Equation 2 the dependence of E on

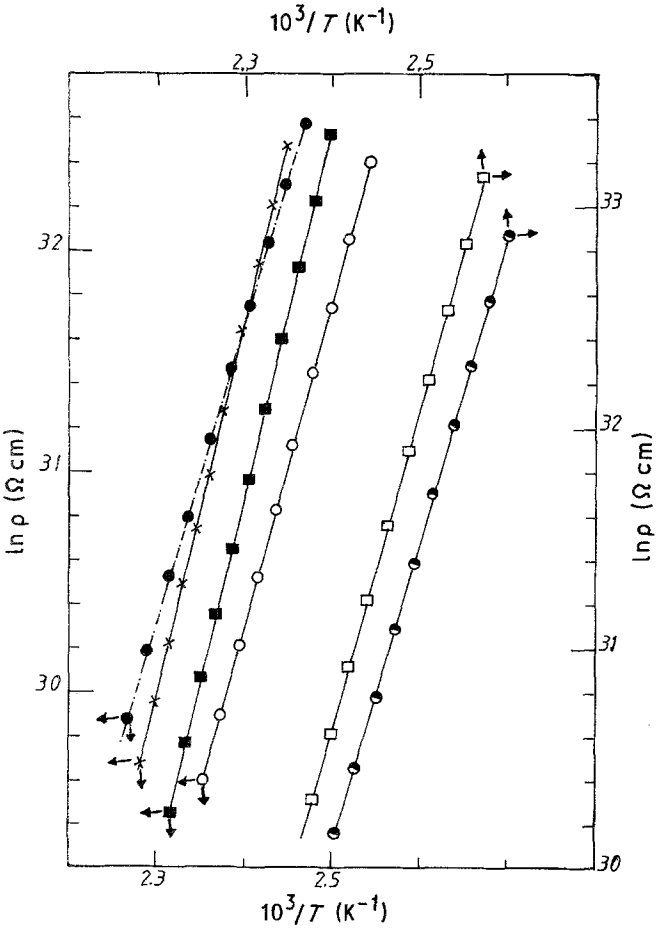

Figure 6 Arrhenius plots for PS loaded with: (●) 2%, (x) 4.5%, (■) 8.5%, (○) 16.5%, (□) 28.5% and (◓) 37.5% Co.

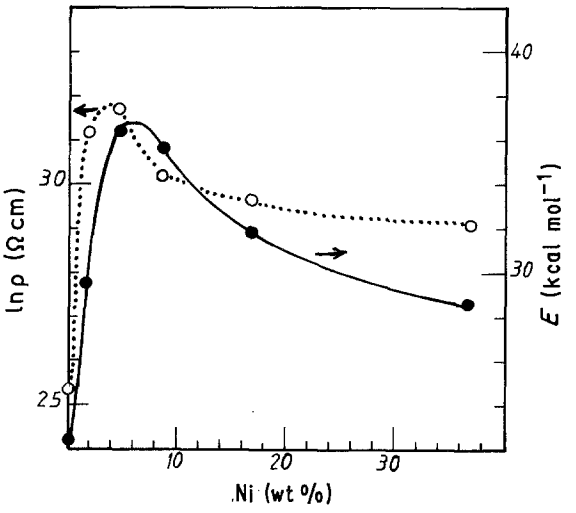

Figure 7 Dependence of ln ϱ and E on the nickel content in PS composites.

the metal content, observed in Figs 7 and 8, can be attributed to the variation of one (or more) of the energies: E_h, E_j and W. It is found that the apparent activation energy E_b, which is equal to $(E_j + W/2\varepsilon)$, is independent of the metal content in the studied range. Thus the change in E is thought to arise mainly from the change in E_h in the following sense. The existence of metallic fillers results in:

(a) the shortening of the main polymeric chain length [12]; and

(b) the formation of a more rigid network in the boundary layer surrounding the filler particle [11]. These two effects may interpret the initial increase of E_h as the metal content increases up to $\simeq 7\%$.

It is noteworthy that the charging energy of a metallic cluster is given by [21]

$$E_c = e^2/2c \qquad (7)$$

where c is the capacitance $\simeq \varepsilon_1 d$, ε_1 ($\simeq 10$) is the effective dielectric constant of the granular metal of grain size $d \simeq 50\,\mu$m. Thus $E_c \simeq 0.07\,\text{kcal mol}^{-1}$, which is a

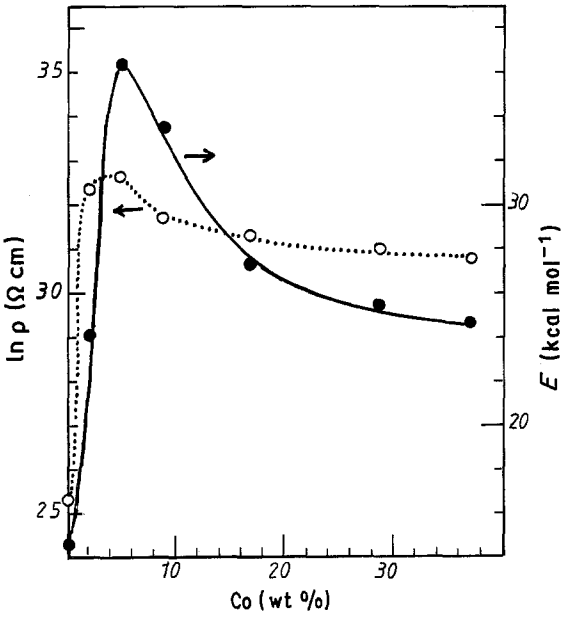

Figure 8 Dependence of ln ϱ and E on the cobalt content in PS composites.

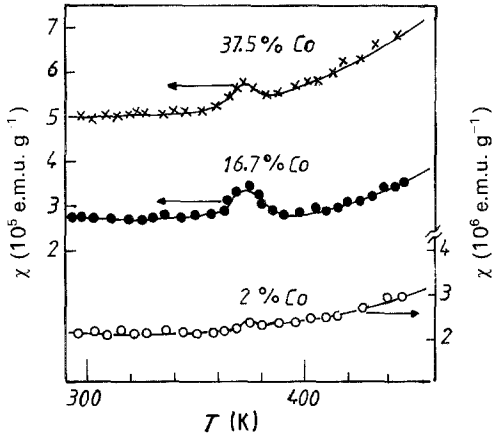

Figure 9 Temperature dependence of χ of PS composites containing cobalt.

very small value. Therefore, the metallic clusters can easily be charged in the presence of the external electric field. As the concentration of these charged clusters increases ($> 7\%$) the intergranular distance (S) > may be reduced to such an extent that the local electrostatic fields cannot be neglected. Warren and Cuthroll [22] proved that the electrostatic force (F), between two conducting spheres (each of radius R) at a constant potential difference, increases by one order of magnitude as $S/2R$ decreases from 10^{-2} to 2×10^{-3}. This finding may attribute the observed decay of the values of E for metallic contents $> 7\%$ in Figs 7 and 8. Morreover, the observed decay of E may be classified into two regions: (a) a relatively sharp decay region (where $7 \lesssim M \lesssim 18\%$), and (b) a region of slight decay in E values (where $M > 18\%$). This slight decay may arise from the enhanced role of the induced volume charge distribution, due to Maxwell Wagner Sillar's polarization [23], around the metallic clusters.

3.4. Magnetic properties

The temperature dependence of the magnetic susceptibility (χ) for the PS composites are plotted in Figs 9 and 10. The plots exhibit the following features.

(a) A slight temperature-dependent character of χ is observed for nickel contents $\geqslant 60\%$ over all the studied temperature range. This character extends only to a temperature close to T_g in the cases of metal contents $\leqslant 37.5\%$, and for these cases

(b) χ exhibits a maximum around T_g and

(c) χ increases pronouncedly as T increases above T_g. It is noteworthy to mention that the pure PS is a diamagnetic material. All of the above results suggest a magnetic role of the polymeric matrix due to the collective states of the π-electrons (magnetic solitons) in the presence of the ferromagnetic metallic clusters.

The probable coupling between the cluster spin, S_n, localized at points x_n ($n = 1, \ldots, N$) along the chain, and the spin, s_n, of π-electrons at the nth impurity (the ferromagnetic cluster in the present case) site may be described by the interaction Hamiltonian of the s–d type

$$H_{s\text{-}d} = J \sum_{n=1,\ldots,N} S_n s_n \qquad (8)$$

which was previously applied in the Su–Schrieffer–

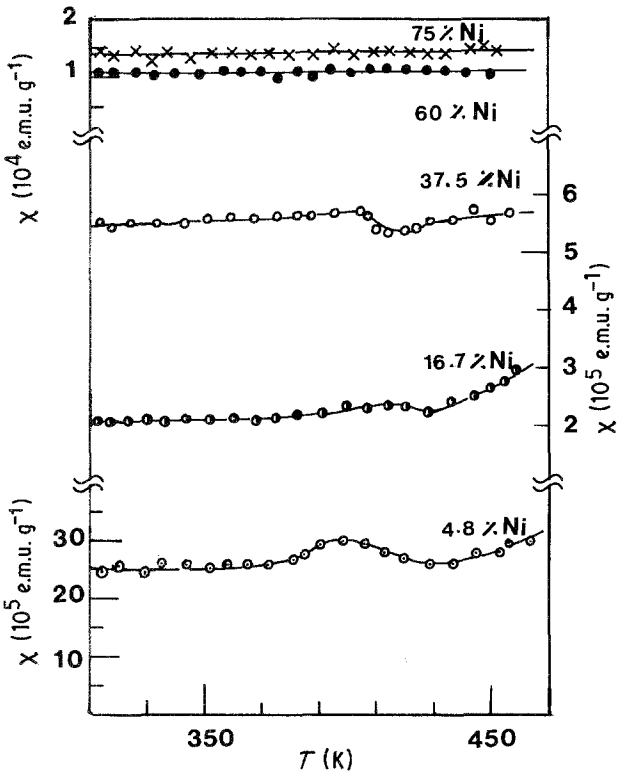

Figure 10 Temperature dependence of χ for PS containing nickel.

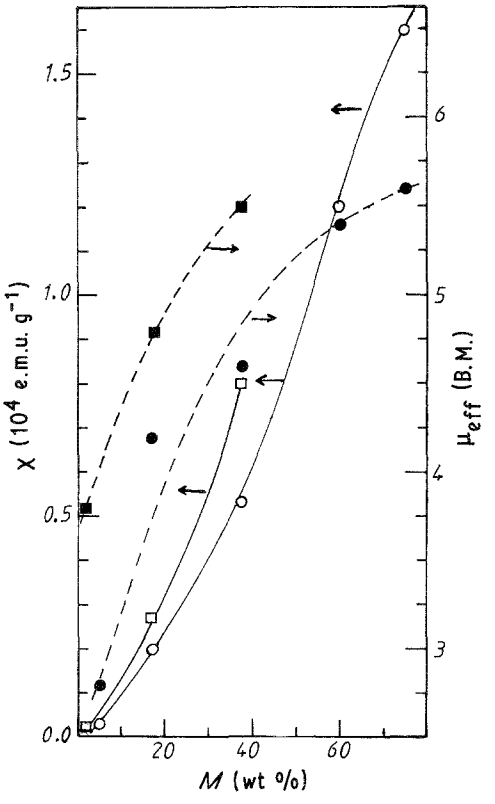

Figure 11 Dependence of χ (at room temperature) and μ_{eff} on (○, ●) nickel and (□, ■) cobalt contents.

Heeger model [24], where J is the exchange energy of interaction. The presence of a magnetic impurity does not change the form of the soliton but changes its energy, and the configurational energy (ε) is given by [25]

$$\varepsilon = E_{Gs} + E_s + (J\sigma_s\sigma_l)/(4\pi \cosh [(x_l - x_s)/\xi_s]) \quad (9)$$

where E_{Gs} is the energy of the ground state, E_s is the energy of the magnetic soliton in the impurity-less case, the soliton spin $\sigma_s = \pm 1$, x_s is the soliton centre, ξ_s is the soliton width [26], σ_l is the magnetic impurity type which does not introduce an extra charge in the chain besides its own spin.

From Equation 9 it follows that when the soliton is far from the impurity (when $|x_l - x_s| \gg \xi_s$), then the soliton is attracted exponentially to the impurity if $(J\sigma_s\sigma_l) < 0$. When the distance $|x_l - x_s|$ is smaller, the interaction, which is always attractive for $(J\sigma_s\sigma_l) < 0$, becomes that of a harmonic oscillator [25]

$$\varepsilon(x_l = x_s) \equiv \varepsilon_s = E_{Gs} + E_s - |J|/(4\pi) \quad (10)$$

$$\varepsilon(x_l - x_s) = \varepsilon(x_l = x_s) + |J|(x_l - x_s)^2/(8\pi\xi_s^2)$$

Thus the soliton becomes pinned to the spin impurity for energetical reasons if $(J\sigma_s\sigma_l)$ is negative. The ferromagnetic coupling ($J < 0$) leads to the minimum of the energy, Equation 10, corresponding to $\sigma_s = \sigma_l$. The total effective spin of the chain plus magnetic impurity has a value of 1. The characteristic frequency of oscillations of the centre of the soliton around the spin impurity is $w = (|J|/2\pi\xi_s M_s)^{1/2}$ where M_s is the mass of the soliton [24]. The measurements of this frequency should give information about the exchange energy, J.

The state with a single magnetic soliton in the presence of a single magnetic impurity becomes thermodynamically more stable than the pure dimerized state without a soliton whenever the exchange energy is larger than the critical value J_c given by

$$J_c = 4\pi E_s \quad (11)$$

The added metallic clusters in the present case of ferromagnetic coupling, enhance the soliton spin in the close vicinity of the cluster surface. The findings of this model can attribute the observed increase of χ, Figs 9 and 10, as T increases (in the polymeric state). The observed peak of χ at T_g supports the role of the polymeric state as a matrix through which the ferromagnetic exchange interaction may proceed.

In the case of Ni $\geqslant$ 60% it is thought that the average distance between the nickel clusters is so short that the cluster–cluster interaction is much stronger than the cluster–soliton interaction. Thus the predominant behaviour does not depend on the polymeric matrix. This may interpret the slight dependence of χ on T and the disappearance of the χ maximum for the cases of Ni $\geqslant$ 60%.

Furthermore, the observed slight temperature dependence of χ in the glassy state, below T_g, suggests a magnetic dilution phenomenon. This means that the added ferromagnetic clusters interact with each other through a nonmagnetoactive matrix. Fig. 11 depicts the dependence of χ (measured at 310 and 300 K) and the effective magnetic moment (μ_{eff}) on nickel and cobalt contents, respectively. These plots agree with the magnetic dilution behaviour. The following equation was used to calculate μ_{eff}

$$\mu_{eff} = 2.84(\chi_m T)^{1/2} \quad (12)$$

where χ_m is the molar susceptibility per magnetic

element. For metallic contents $\leqslant 37.5\%$ the obtained values of μ_{eff} are less than the theoretically calculated moments, which are typically 5.56 and 6.56 B.M. (Bohr Magniton) for Ni^{2+} and Co^{2+}, respectively. On the other hand, the obtained values of μ_{eff} for nickel contents $\geqslant 60\%$ are very close to the corresponding theoretical value. These results confirm the assumption that for high contents of nickel the main ferromagnetic coupling is due to the nickel clusters with no pronounced role of the polymeric matrix.

4. Conclusions

It may be concluded that the variation of ϱ (as a function of metal content, M) follows the variation of E, which arose mainly from the change in E_h. The local electrostatic fields, between the charged metallic clusters affect E for $7 \leqslant M \leqslant 18\%$. The induced volume charge distributions, due to Maxwell Wagner Sillar's polarization, play a reasonable role at $M > 18\%$. A ferromagnetic interaction is thought to proceed between the metallic clusters and the magnetic solitons, within the polymeric matrix in the close vicinity of the cluster surface. At $M \geqslant 60\%$ the cluster–cluster ferromagnetic interaction predominates.

References

1. B. WUNDERLICH, D. M. BODILY and M. H. KAPLAN, *J. Appl. Phys.* **35** (1964) 95.
2. P. DESTRUEL and H. T. GIAM, *J. Polym. Sci. Polym. Phys. Edn* **21** (1983) 851.
3. E. MARCHAL, H. BENOIT and O. VOGL, *ibid.* **16** (1978) 949.
4. L. H. WANG and R. S. PORTER, *ibid.* **21** (1983) 907.
5. M. A. KENNEDY, G. TURTURRO, G. R. BROWN and L. E. ST-PIERRE, *ibid.* **21** (1983) 1403.
6. C. S. HENKEE and E. J. KRAMER, *ibid.* **22** (1984) 721.
7. J. LUCKI, J. F. RABEK, B. RANBY and Y. C. JIANG, *Polymer* **27** (1986) 1193.
8. A. TAWANSI, M. D. MIGAHED and M. I. A. EL-HAMID, *J. Polym. Sci. Polym. Phys. Edn* **24** (1986) 2631.
9. A. TAWANSI, PhD thesis, Moscow State University (1977).
10. A. TAWANSI, M. D. MIGAHED and M. I. A. EL-HAMID, *Phys. D Appl. Phys.* **20** (1987) 766.
11. W. SCHEIBNER and M. JÄCKEL, *Phys. Status Solidi (a)* **87** (1985) 543.
12. M. PINHEIRO and H. M. ROSENBERG, *J. Polym. Sci. Polym. Phys. Edn* **18** (1980) 217.
13. J. N. GOODIER, *J. Appl. Mech.* **1** (1933) 39.
14. M. KALNIN and D. T. TURNER, *J. Mater. Sci. Lett.* **4** (1985) 1476.
15. P. HEDVIG, "Dielectric spectroscopy of polymers" (Hilger, Bristol, 1977) pp. 76.
16. O. YANO and Y. WADA, *J. Polym. Sci.* **A-2** (1971) 669.
17. B. WUNDERLICH and D. M. BODILY, *J. Appl. Phys.* **35** (1964) 103.
18. T. MIYAMOTO and K. SHIBAYAMA, *ibid.* **44** (1973) 5372.
19. S. GLASSTON and H. EYRING, "The theory of rate process" (McGraw-Hill, New York, 1947).
20. R. E. BARKER, J. R. THOMAS and C. R. THOMAS, *J. Appl. Phys.* **35** (1964) 3203.
21. K. K. THORNBER, T. C. McGILL and C. A. MEAD, *ibid.* **38** (1967) 2384.
22. W. E. WARREN and R. E. CUTHROLL, *ibid.* **46** (1975) 4598.
23. A. GARCIA, C. GROSSE and P. BRITO, *J. Phys. D Appl. Phys.* **18** (1985) 739.
24. W. P. SU, J. R. SCHRIEFFER and A. J. HEEGER, *Phys. Rev. B* **22** (1980) 2099.
25. O. HUDAK, *Czech. J. Phys.* **B35** (1985) 1303.
26. J. HARA and H. FUKUYAMA, *J. Phys. Soc. Jpn* **52** (1983) 2128.

Rceived 26 April
and accepted 8 September 1988